applied sciences

MDPI

Article

Enhanced Heterogeneous Activation of Peroxymonosulfate by Nitrogen–Sulfur Co-Doped Mofs-Derived Carbon

Chuning Zhang, Huaqiang Chu, Qian Ma, Yanyan Chen and Jianwei Fan *

School of Environmental Science and Engineering, Tongji University, Shanghai 200092, China
* Correspondence: fanjianwei@tongji.edu.cn

Abstract: It is important to further enhance the performance of green and efficient non-homogeneous catalysts for advanced oxidation process of Peroxymonosulfate (PMS-AOP) for green treatment of industrial wastewater. In this paper, nitrogen–sulfur co-doped MOFs-derived carbon material (CoSN@C) was prepared by one-pot synthesis followed by carbonization, and its morphological structure was characterized by XRD and SEM. After pyrolysis, the CoSN@C still maintained the dodecahedral morphology and structure of ZIF-67. The synergistic effects of S and N significantly elevated the activation of PMS. The results show that the CoSN@C + PMS system can effectively activate PMS to degrade Rhodamine B (RhB), with a rate constant (1.85 min^{-1}) four times higher than that of the CoN@C + PMS system (0.44 min^{-1}). The optimal catalytic process parameters of material dosage, PMS concentration, temperature, pH, and other parameters were also investigated for the activation of PMS to remove Rhodamine B. The cyclic experiment shows that the CoSN@C has excellent recyclability and the degradation rate of RhB still reached 88.9% after four cycles. Radical capture experiments and EPR tests showed that the CoSN@C + PMS system generated a large amount of $SO_4 \cdot^-$ and ·OH radicals adsorbed on the catalyst surface and a certain amount of singlet oxygen, and the free radical pathway and non-radical pathway worked together to degrade RhB efficiently and rapidly. While non-radical pathway with singlet oxygen as main reactive oxygen species played a key role in the CoN@C + PMS system. This work provides a new idea for the rational design of non-homogeneous catalysts for PMS-AOP system.

Keywords: advanced oxidation process; peroxymonosulfate (PMS); non-homogeneous catalyst; MOFs

Citation: Zhang, C.; Chu, H.; Ma, Q.; Chen, Y.; Fan, J. Enhanced Heterogeneous Activation of Peroxymonosulfate by Nitrogen–Sulfur Co-Doped Mofs-Derived Carbon. *Appl. Sci.* **2023**, *13*, 3182. https://doi.org/10.3390/app13053182

Academic Editors: Petr Korusenko and Sergey Nesov

Received: 28 December 2022
Revised: 23 February 2023
Accepted: 28 February 2023
Published: 1 March 2023

1. Introduction

With the expansion of contemporary industry, the problem of polluted industrial wastewater is getting more severe, and untreated pollutants can enter the environment via a variety of routes and impair the health of living beings [1]. Among these, dye wastewater is difficult to biodegrade due to its enormous stock, weak biochemical characteristics, and complicated composition [2]. Rhodamine B (RhB) is extensively investigated as a model contaminant for the treatment of dye effluent. It is found in wastewater from the textile, cosmetic, and food industries, and is on the World Health Organization's list of carcinogens in Class III [3–6].

The advanced oxidation process based on peroxymonosulfate (PMS-AOP) is used to treat resistant wastewater [7]. Peroxymonosulfate (PMS) is stable under normal settings, and ROC are produced slowly. Previous research showed chloride ion (Cl^-), organic ligand with reducing capability, and microwave (MW) heating, was introduced into AOP for enhanced removal of organic contaminants in wastewater [8–11]. Due to their gentle reaction conditions, high ROC generation rate, and low energy consumption, PMS-AOP focuses on transition metal-based catalysts to catalyze PMS [12]. Improving transition metal oxide dispersion to minimize agglomeration and boosting activated PMS efficiency are key research areas [13,14]. Zeolitic Imidazolate Frameworks (ZIFs), like normal MOFs, are widely employed in adsorption, separation, and catalysis [13–15]. MOF-derived carbon

is employed in adsorption, catalytic gas reactions, and fuel cell construction. MOF-derived carbon materials can activate PMS to generate reactive oxygen species for treating refractory organic contaminants in wastewater due to the presence of transition metals such as Fe and Co in their structure and heteroatom (nitrogen and sulfur) doping [16–20]. Numerous studies have shown that sulfur doping can change the electron distribution of nitrogen-doped carbon materials, which facilitates the catalytic process and provides stability [21–23]. The process of synthesizing simple and large quantities of materials that change the electron distribution of carbon materials by introducing sulfur doping for efficient catalytic persulfate activation deserves further investigation.

In this study, the sulfur-functionalized MOFs precursor ZIF-67-S was synthesized with allylthiourea utilizing a one-pot technique. Co-doped sulfur–nitrogen porous carbon materials (CoSN@C) were produced by roasting in N_2 atmosphere. Their performance in catalyzing the degradation of Rhodamine B (RhB), a common dye, by PMS was studied, and their structure and morphology were characterized. The experimentally prepared CoSN@C inherited the MOFs precursor's well-dispersed and porous three-dimensional spatial structure. The complete contact with PMS and sulfur doping further enhanced its catalytic ability, and the material demonstrated outstanding performance in activating PMS degradation of pollutants. In addition, the experiments investigated the effects of material dosing amount, PMS dosing concentration, temperature, pH, and other parameters on the RhB degradation effect to determine the optimal conditions for degradation. The catalytic degradation mechanisms of CoSN@C + PMS system and CoN@C + PMS system were compared through quenching experiments and electron paramagnetic resonance (EPR) tests to identify the effect of S doping.

2. Materials and Methods

2.1. Chemical Materials

2-Methylimidazole, allyl thiourea, sulfuric acid (H_2SO_4), sodium hydroxide (NaOH), sodium carbonate (Na_2CO_3), sodium dihydrogen phosphate (NaH_2PO_4), sodium sulfate anhydrous (Na_2SO_4), sodium hydrogen carbonate ($NaHCO_3$), sodium nitrate ($NaNO_3$), sodium chloride (NaCl), furfuryl alcohol (FFA), p-benzoquinone (p-BQ), L-Histidine and methanol (MeOH) were purchased from Sinopharm Chemical Reagent Co., Ltd., Shanghai, China, Peroxymonosulfate (PMS, $KHSO_5{\cdot}0.5KHSO_4{\cdot}0.5K_2SO_4$), cobaltous nitrate hexahydrate ($Co(NO_3)_2{\cdot}6H_2O$), 1-allyl-2-thiourea($C_4H_8N_2S$), bisphenol-A (BPA), 4-chlorophenol (4-CP), nitrobenzene (NB), methyl phenyl sulfoxide (PMSO), and rhodamine B (RhB) were purchased from Aladdin Chemical Co., Ltd.

2.2. Synthesis of Catalysts

2.2.1. Preparation of Sulfur-Containing Precursor ZIF-67-S

Amounts of 1.455 g $Co(NO_3)_2{\cdot}6H_2O$ and 1.65 g 2-methylimidazole were dissolved in 20 mL of methanol, and 3 g allylthiourea was dissolved in 60 mL of methanol. Then, the obtained $Co(NO_3)_2{\cdot}$solution and 2-methylimidazole solution were poured into 60 mL of allylthiourea in methanol and stirred for 12 h at room temperature. The obtained sulfur-containing ZIF-67-S precursor powder was washed by centrifugation in methanol three times, dried at 60 °C overnight under vacuum and collected.

2.2.2. Preparation of Sulfur-Containing Precursor ZIF-8-S

Next, 0.746 g $Zn(NO_3)_2{\cdot}6H_2O$ was dissolved in 24.5 mL MeOH and 1.65 g 2-methylimidazole was dissolved in 30 mL MeOH, and the subsequent operation was the same as Section 2.2.1. to obtain the sulfur-containing precursor powder of ZIF-8-S without Co.

2.2.3. Preparation of Precursor ZIF-67

The obtained $Co(NO_3)_2$ MeOH solution and 2-methylimidazole methanol solution were poured into 60 mL of methanol and stirred at room temperature for 12 h. Other operations were performed as in Section 2.2.1. to obtain the ZIF-67 precursor powder without sulfur.

2.2.4. Preparation of CoSN@C, CoN@C and SN@C

The dried precursors ZIF-67-S, ZIF-8-S, and ZIF-67 were subjected to thermal treatment at 1 °C·min^{-1} temperature ramp rate in N_2 atmosphere. The temperature rose to 900 °C and maintained for 1 h, and the final obtained samples were named CoSN@C, SN@C, and CoN@C, respectively.

2.3. Experimental Procedures

The degradation experiments were conducted at room temperature, and 50 mL RhB solution (20 mg L^{-1}) was added to the glass bottle. Catalysts (0.05 mg L^{-1}) and PMS (1 mM) solution were added to initiate the reaction, while the solution was kept homogeneous by constant stirring. At given time intervals, samples were collected and filtered through a 0.22 μm filter, then quenched with excess $Na_2S_2O_3$ solution for RhB analysis by UV-vis spectrophotometer to determine the concentration of RhB.

The pH values of the solution were adjusted by 0.1 M perchloric acid (if needed), 0.01 M acetate buffer (if needed), and 0.01 M borate buffer (if needed). The reaction temperature was changed with a thermostatic water bath system (if needed). Next, 10 mM of different anions (Cl^-, NO_3^-, HCO_3^-, and $H_2PO_3^-$) were added to demonstrate their influence on the process. A certain amount of different quenchers (MeOH, TBA, FFA, and PMSO) was added separately to investigate the effect of different reactive oxygen species on degradation during the reaction. The CoSN@C was evaluated through five cycles to investigate the Stability of catalysts. After the reaction was completed, the catalyst was washed with anhydrous EtOH and deionized water and centrifuged three times at 9000 r min^{-1}, after which the catalyst was dried under vacuum at 60 °C for the next degradation experiment.

2.4. Material Characterization and Analytical Methods

The concentration of RhB was measured by UV-vis spectrophotometer (Shimadzu UV2550, Kyoto, Japan) with absorbance at 554 nm. Scanning electron microscope (SEM, ZEISS Gemini 300, Jena, Germany) was used to investigate the morphology, coupled with Energy disperse spectrometer (EDS) mapping to determine the elemental compositions. The microstructure of the materials was characterized by transmission electron microscopy (TEM, FEI Tecnai 12, Hillsboro, OR, USA). The crystalline structure of the catalysts was determined by X-ray diffraction (XRD, Bruker D8 Adance, Heidelberg, Germany) with Cu Kα radiation. The states of elements and elemental valence of the material before and after the reaction were determined by X-ray photoelectron spectrometer (XPS, Thermo Scientific Nicolet iS5, Waltham, MA, USA). Electron paramagnetic resonance (EPR, Bruker EMXplus-6/1, Heidelberg, Germany) spectroscopy was employed to in detect the generated ROS. The Brunauer-Emmett-Teller (BET) specific surface area was measured through analyzing the N_2 adsorption-desorption isotherm (Micromeritics ASAP 2460, Norcross, GA, USA). The total organic carbon (TOC) of the solution was tested on a Thermo Scientific Vario TOC (Waltham, MA, USA).

3. Results

3.1. Characterization of CoSN@C

The SEM data allow for the observation of the material's surface morphology (Figure 1a,b). Figure 1a,c are SEM images of the CoN@C carbon-derived material used as the control. The pyrolyzed CoN@C nanoparticles retain their homogeneous dodecahedral morphology and structure, with an average diameter of around 500 nm and a wrinkled surface.

Figure 1b,d are SEM images of the CoSN@C carbon-derived materials after sulfur modification. Moreover, Figure 1b demonstrates that the majority of the CoSN@C nanoparticles after pyrolysis still have dodecahedral morphology and structure with an average diameter of about 600 nm, with a certain degree of aggregation and fragmentation and obvious pores, most likely due to the high-temperature pyrolysis. The high-temperature pyrolysis of allylthiourea employed for sulfur modification may result in structural fragmentation and the formation of pores, which makes it possible for a larger area to adsorb pollutants, and is advantageous for PMS activation. The elements of S, Co, C, N, and O were uniformly distributed in the catalysts, according to the EDS mapping data (Figure 1g,h). TEM was used to explore the material's structure in further detail (Figure 1e,f). The nanoparticles were contained in the carbon layer, according to the TEM image. The nanoparticles were dispersed on the carbon layer's surface and were contained in it, according to TEM pictures.

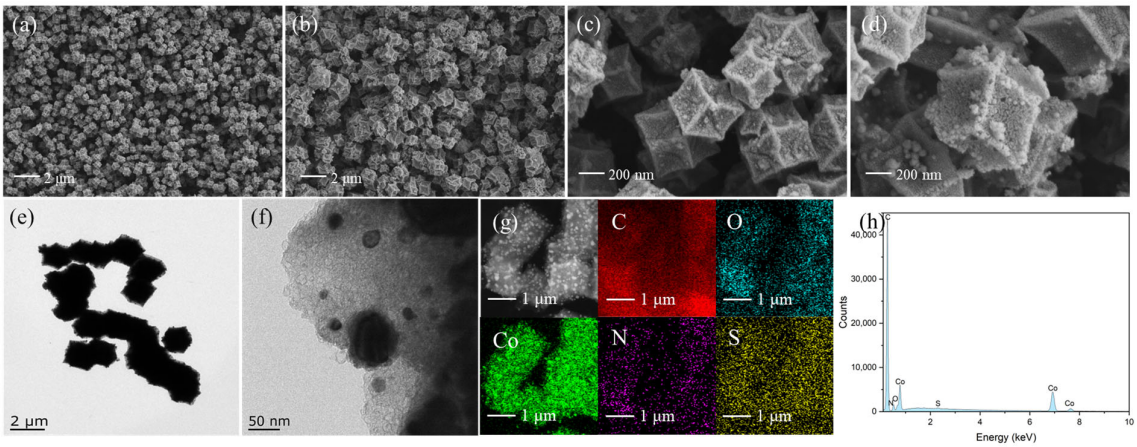

Figure 1. SEM images of CoN@C (**a**,**c**); SEM images of CoSN@C (**b**,**d**); TEM images of CoSN@C (**e**,**f**); SEM image of CoSN@C and corresponding elemental mappings of C, N, O, S, and Co elements (**g**); EDS of CoSN@C and X-ray maps of C, N, O, S, and Co (**h**).

By using XRD, the produced material's crystal structure was examined. According to prior investigations, ZIF-67 was present in the unpyrolyzed catalysts as evidenced by the XRD patterns of the unpyrolyzed material ZIF-67 and ZIF-67-S, which exhibited three diffraction peaks of ZIF-67 at 7.19°, 10.34°, and 12.82°, respectively (Figure 2a) [24–26]. Compared to pure ZIF-67, the XRD patterns of ZIF-67-S exhibited broader diffraction peaks and decreased intensity of diffraction peaks. The direct synthesis of thiourea-functionalized organic frameworks (S-MOFs), as described in the literature, can influence the porosity, crystallinity, and stability of the materials via various types of secondary interactions [27,28]. In this study, the crystallinity of ZIF-67-S decreased following sulfur doping modification by thiourea-functionalized MOFs, as determined by a combination of XRD and SEM data. Both CoN@C and CoSN@C are derived by pyrolysis in an inert gas atmosphere. The XRD patterns of the CoN@C and CoSN@C catalysts represented a diffraction peak located at 44°, 52°, and 76°, corresponding, respectively, to the (111), (200), and (220) planes of metal Cobalt, implying the reduction in cobalt monomers dispersed in the carbon frameworks after pyrolysis at 900 °C (Figure 1b) [29,30], thus verifying that the small particles on the surface of the samples shown by SEM results are metallic cobalt monomers. Comparatively, the XRD pattern of CoN@C and CoSN@C revealed the presence of g-N3C4 (JCPDS PDF#87-1525) (Figure 2b), which indicates a high degree of graphitization [31], which is advantageous for the activation of PMS [32,33].

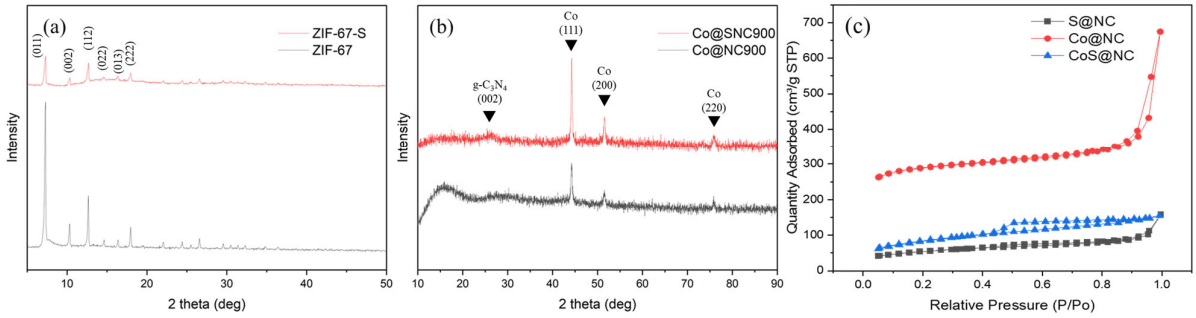

Figure 2. XRD patterns of ZIF-67 and ZIF-67-S precursors (**a**); CoN@C and CoSN@C (**b**); nitrogen adsorption and desorption isotherms for SN@C, CoN@C, and CoSN@C (**c**).

The nitrogen adsorption–desorption isotherm (Figure 2c) showed that when $p/p_0 > 0.2$, the amount of nitrogen adsorbed by the aforementioned materials increased gradually, whereas CoN@C and CoSN@C showed a hysteresis loop in the adsorption isotherm, indicating the presence of mesopores. According to the results of nitrogen sorption, SN@C exhibits type I isotherms. Additionally, the nitrogen adsorption isotherm of CoN@C and CoSN@C were comparable to type-IV(H_2) and type-IV, respectively (H4). The BET surface areas of SN@C, CoN@C, and CoSN@C were 185.02 $m^2\ g^{-1}$, 876.66 $m^2\ g^{-1}$, and 293.30 $m^2\ g^{-1}$, respectively. The samples' pore volume and size were displayed in Table 1. The direct synthesis of S-MOFs can influence the porosity after pyrolysis process; therefore, the surface of CoSN@C began to contract while the pore size and the pore volume dropped in comparison to the CoN@C.

Table 1. Surface area, pore size, and pore volume parameters of SN@C, CoN@C and CoSN@C.

Catalysts	Surface Area ($m^2\ g^{-1}$)	Pore Size (nm)	Pore Volume ($cm^3\ g^{-1}$)
CoSN@C	293.30	3.26	0.24
CoN@C	876.66	4.76	1.04
SN@C	185.02	5.23	0.24

3.2. Catalytic Activity of CoSN@C

To test the catalytic activity of the synthesized catalyst, RhB was chosen as a model pollutant, and the comparative performance of SN@C, CoN@C, and CoSN@C for the degradation of RhB by PMS was examined. Figure 3a shows the degradation of RhB by several catalytic systems. In the experiment, the initial concentration of RhB was 20 mg L^{-1}, the concentration of PMS was 1 mM, the initial pH of the reaction system was 5 after adding PMS, and the reaction temperature was approximately 20 °C. RhB concentration decreased minimally when only PMS was employed, showing that PMS self-activation's effect on creating reactive radicals was minimal [34,35]. With SN@C + PMS, CoN@C + PMS, and CoSN@C + PMS, the RhB degradation rates reached 34.0%, 66.0%, and 99.5% in 3 min 44.5%, 92.3%, and 100% in 4 min, respectively. Both the introduction of sulfur modification and Co loading on MOFs-derived carbon exhibited strong activation properties for PMS, with Co loading on sulfur carbide-modified MOFs achieving the best RhB degradation with CoSN@C. Meanwhile, Figure 3b showed the adsorption equilibrium of CoSN@C for RhB was reached within 30 min. Moreover, ~40% of TOC was removed after 10 min reaction (Figure 3d). To further study the kinetic characteristics of SN@C, CoN@C, and CoSN@C on the RhB degradation reaction, a fit was performed using Equation (1) for the primary reaction kinetic model:

$$ln\left(\frac{C_a}{C_0}\right) = -kt \quad (1)$$

where C_0 (mg L^{-1}) and C_a (mg L^{-1}) are the initial RhB concentration and RhB concentration at moment a (min), k is the primary reaction rate constant (min^{-1}), and t is the reaction time (min).

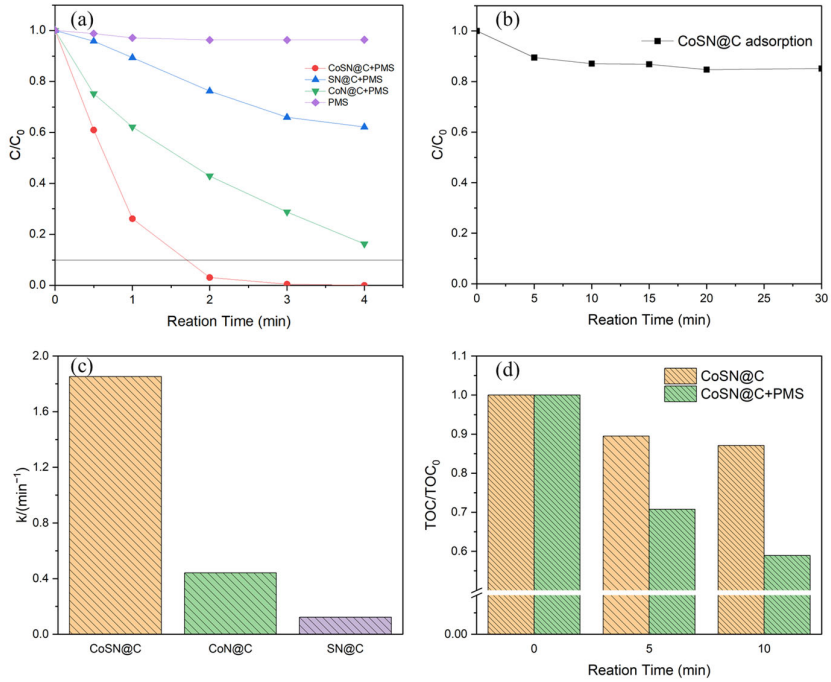

Figure 3. Comparison of degradation performance in different system (**a**); adsorption process of CoSN@C (**b**); the calculated pseudo-first-order rate constants (k) for RhB degradation (**c**); and TOC removal in the CoSN@C + PMS and CoSN@C system (**d**).

According to Table 2, the apparent reaction rate constants (k) for RhB degradation by SN@C, CoN@C, and CoSN@C as catalysts for activated PMS were 0.122 min^{-1}, 0.442 min^{-1}, and 1.852 min^{-1}, respectively. CoSN@C activated PMS was the most rapid of the materials, with an apparent reaction rate constant (k_{app}) 4.2 times greater than CoN@C and 15.2 times greater than SN@C. The N site, C site, and S site performances alone have limited ability to activate PMS. In contrast, the active site containing Co is the key that can efficiently activate PMS and generate reactive oxygen species to degrade RhB. The Co-containing active sites synergistic with S-doping can activate PMS to degrade organic matter more efficiently [36].

Table 2. RhB degradation kinetics fitted by the pseudo-first-order reaction.

Catalysts	k/(min^{-1})	R^2
CoSN@C	1.852	0.99
CoN@C	0.442	0.98
SN@C	0.122	0.99

Figure 4a exhibits the RhB degradation efficiency at various PMS molar concentrations. The RhB degradation rates at 4 min were 95.52%, 100%, and 97.76% when the PMS molar concentrations were 0.5 mM, 1 mM, and 2 mM, respectively. When the PMS molar concentration was above 1 mM, the growing trend of the RhB degradation rate slowed, which shows that there is also an optimum value for PMS concentration. The addition of excess PMS may produce excess sulfate radicals, not only leading to react with itself, but also be consumed by excessive PMS to ROS with lower oxidation capacity [37]. For future studies, a 1 mM PMS molar concentration was selected. The effect of the change in catalyst dosage on the RhB degradation rate was evaluated, and the results are depicted in Figure 4b. When the catalyst dosage of CoSN@C was 0 mg L^{-1}, 0.025 mg L^{-1}, 0.05 mg L^{-1}, and 0.1 mg

L^{-1}, the degradation rates of RhB were 3.64%, 90.10%, 100%, and 100%, respectively. The degradation efficiency increases with the increase in catalyst dosage due to the increased number of catalytic sites and the probability of contact between active sites and PMS. Considering economic reasons, the optimal dosage of catalyst and PMS was determined to be 0.05 mg L^{-1} and 1 mM, respectively.

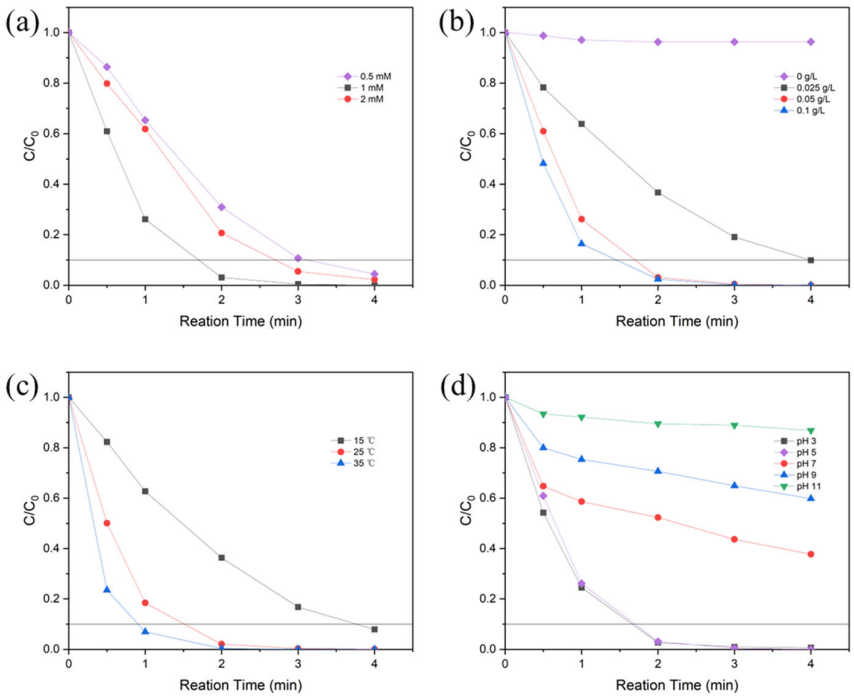

Figure 4. Effects of some operating parameters on the degradation phenol by CoSN@C + PMS system: (**a**) PMS dosage; (**b**) catalyst loading; (**c**) temperature; and (**d**) initial pH.

Figure 4c shows, when the reaction temperatures were 15 °C, 25 °C and 35 °C, the degradation rates of RhB for 4 min were 92.08%, 99.92%, and 100.00%, corresponding to the degradation reaction rate constants (k) of 0.65 min^{-1}, 1.85 min^{-1}, and 2.83 min^{-1}, respectively, and the degradation rates accelerated with the increase in reaction temperature. Figure 3d shows the effect of pH change from 3.0 to 11.0 on the degradation of RhB by CoSN@C + PMS system. The catalyst is effective under acidic conditions when the pH is 3–5. The degradation rate of RhB can reach 99.9% at 4 min. Furthermore, it becomes less effective under alkaline conditions, which may have been due to a large number of hydroxide ions (HO) in the solution making the surface of CoSN@C material hydroxylated, thus affecting the adsorption of PMS on the surface of the material, which is not conducive to PMS catalytic activation [38]. In addition, PMS undergoes autolysis at higher pH through a non-radical pathway, which also decreases the degradation rate of RhB [39,40]. Therefore, the CoSN@C-PMS catalytic system has the best catalytic effect between pH 3 and 5.

Various inorganic anions in the actual water body influence the activation performance of the catalyst. Common inorganic anions such as Cl^-, NO_3^-, HCO_3^-, and $H_2PO_3^-$ in aqueous humor were chosen to examine the influence of their presence on the catalytic activation of PMS for RhB degradation (Figure 5). When $H_2PO_3^-$ was added to the solution, a significant enhancement of the catalytic system's ability to degrade RhB was observed, and the rate of RhB degradation was close to 100% after 1–2 min of reaction. It may be the dissociation of $H_2PO_3^-$ in solution releasing HPO_3^{2-}, and nucleophilic attack on PMS, enhancing the generation of SO_4^- and $^1O_2$ to improve degradation [41,42]. In contrast, after adding Cl^- and NO_3^-, the RhB degradation rate after 4 min reaction was 97.85 and 99.33%, respectively, with less effect. The addition of HCO_3^- decreased the RhB degradation rate to 71.5%, which significantly inhibited RhB degradation, most likely due to the reaction

of HCO_3^- with singlet oxygen and free radicals to form carbonate radicals with deficient activity [29,43].

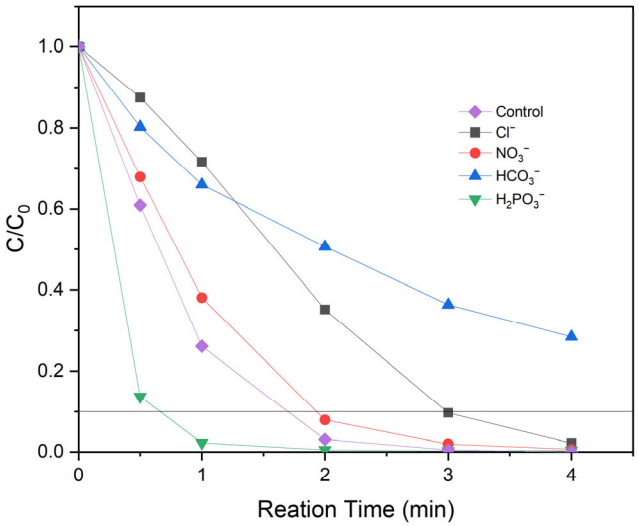

Figure 5. The degradation of RhB on different concentration anions.

3.3. Cycling Stability and Failure Analysis of CoSN@C

After three cycles of experiments, the catalyst could still remove RhB at a rate of 96.15% in 4 min (Figure 6). This value dropped to 88.87% after four cycles and 75.20% after five cycles, suggesting that the CoSN@C catalyst had a strong activation ability for PMS and could be recovered and recycled simultaneously.

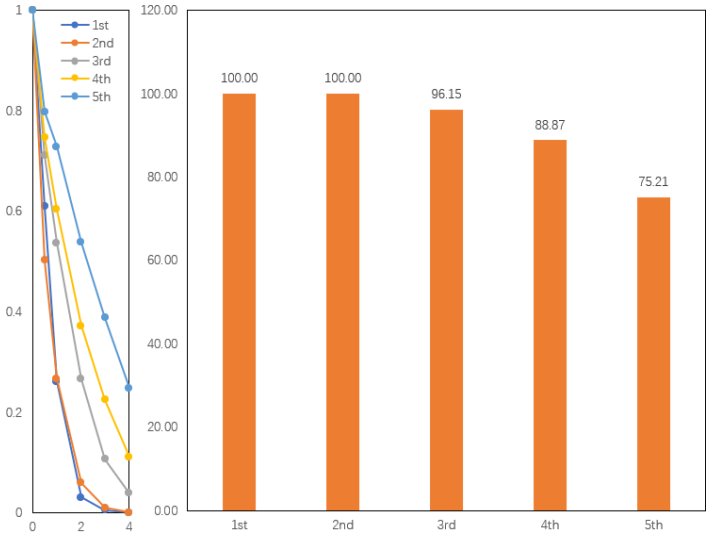

Figure 6. The Circulation experiment of CoSN@C + PMS system on degradation.

To investigate the cause of catalyst failure, the crystal structure of the CoSN@C catalyst before and after use was characterized. The results are displayed in Figure 7, where it can be seen that the crystal structure of the catalyst did not change fundamentally after several cycles of experiments and had structural stability. The (002) diffraction peak of g-N_3C_4 and the (111) crystal plane diffraction peak of cobalt monomer near 44° are still present in the failed CoSN@C material, and the relative intensity of the diffraction peak becomes more pronounced, and the (111) crystal plane diffraction peak of cobalt monomer becomes wider, i.e., the degree of crystallization of cobalt worsens, presumably.

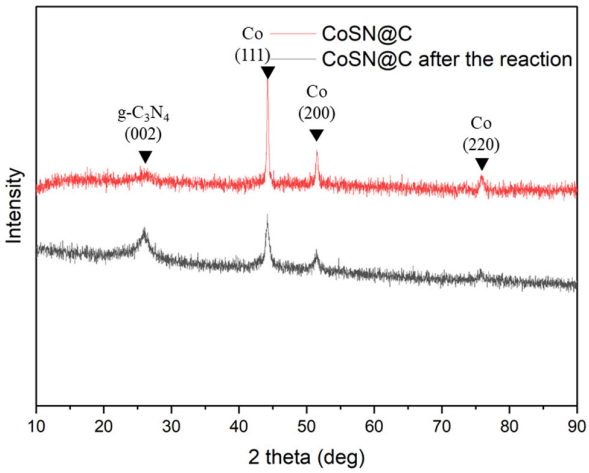

Figure 7. XRD spectra of CoSN@C and CoSN@C after the reaction.

3.4. Identification of Reactive Species and Mechanism

Quenching experiments and EPR tests were conducted to confirm the influence of reactive oxygen species (ROS) in the reaction system of CoN@C + PMS system for RhB degradation. MeOH and TBA were utilized as quenchers for $SO_4 \cdot^-$ and HO· radicals, respectively, PMSO as a quencher for radicals adsorbed on the catalyst surface, and FFA as an quenchers for $^1O_2$ [44]. Figure 8a,b exhibit the variations in the reaction rates of RhB degradation by CoSN@C and CoN@C activated PMS following the addition of various quenchers.

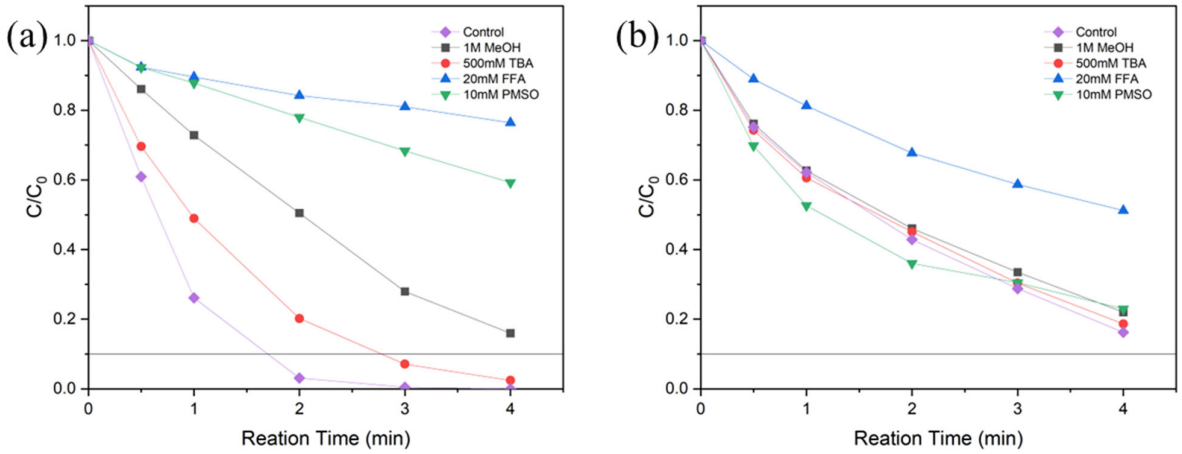

Figure 8. Influence of quenching agents on RhB degradation in the different catalyst/PMS system: (**a**) CoSN@C + PMS; (**b**) CoN@C + PMS.

RhB's degradation efficiency in the CoN@C + PMS system was not significantly altered by adding MeOH, TBA, or PMSO, as compared to the control group's efficiency of 83.77%. However, the degradation rate plummeted dramatically to 48.8% when FFA was added. It indicates that the free and adsorbed $SO_4 \cdot^-$ and HO·radicals on the catalyst surface do not exist in the CoN@C + PMS reaction system, while $^1O_2$ plays a major role in the degradation of RhB in the CoN@C + PMS system. The PMS is oxidized into $\cdot O_2^-$, while $\cdot O_2^-$ is reorganized as an intermediate to produce a large amount of $^1O_2$, which oxidatively degrades RhB, which is consistent with the results of previous studies [21,45,46]. The addition of TBA decreased the RhB degradation rate from 100% in the control group to 97.6%, whereas adding MeOH decreased the RhB degradation rate to 84.0% (Figure 8a). The results demonstrated that both MeOH and TBA inhibited the degradation of RhB, but not to a significant degree, indicating that the reactive oxygen species in the reaction system that played a significant role in the degradation of RhB were not free $SO_4 \cdot^-$ and

free HO·, and that the slight decrease in the reaction rate was likely caused by the addition of alcohols that interfered with the contact between PMS and the active sites on the catalyst surface. $SO_4\cdot^-$ and HO· adsorbed on the catalyst surface played the primary role in the RhB degradation by CoSN@C + PMS system; the RhB degradation was also severely inhibited by the addition of FFA, and the rate decreased to 23.8%. According to literature, FFA can quench $^1O_2$ and has an influence on $SO_4\cdot^-$ and HO·radicals; when combined with the PMSO quenching results, in addition to the $SO_4\cdot^-$ and HO· adsorbed on the catalyst surface, $^1O_2$ may be generated and contribute to the reaction. Consequently, the results of the quenching experiments must be validated using EPR tests on CoSN@C [47].

For electron paramagnetic resonance (EPR) tests, DMPO is commonly used. As shown in Figure 9, compared to the DMPO/PMS system, the addition of CoSN@C resulted in a quadruple peak with a intensity ratio of 1:2:2:1 and a sextuple peak with a intensity ratio of 1:1:1:1:1:1, corresponding to DMPO-HO· and DMPO-$SO_4\cdot^-$, respectively, indicating that CoSN@C has strongly oxidized the $SO_4\cdot^-$ and HO·radicals upon contact with the quadruple peak signal of HO· that was observed in both the DMPO/PMS system and the system with the addition of the catalyst; however, the intensity of the signal in the PMS/DMPO/CoSN@C system was significantly higher than that in the PMS-only system, indicating that the content of HO· was substantially increased in the system with the addition of the catalyst and that the weak quadruple peak signal in the PMS solution alone was due to the autodecomposition of PMS [36].

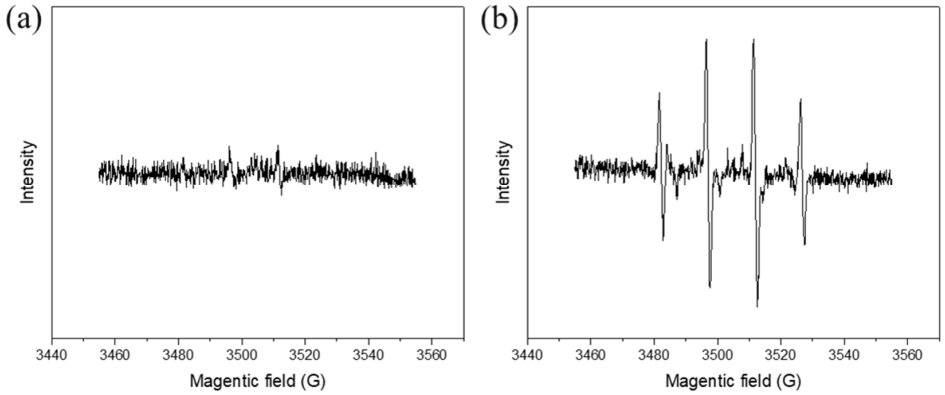

Figure 9. Identification of radical: (**a**) EPR spectra without catalyst; (**b**) EPR spectra with catalyst.

Figure 10 displays the outcomes of using TEMP as the spin-trapping agent to confirm the presence of the non-radical species $^1O_2$. Since there was no TEMP$-^1O_2$ signal for the PMS/TEMP system, the presence of reaction-generated $^1O_2$ in the system was confirmed. A triple peak signal with the ratio of 1:1:1 was seen for the PMS/TEMP/CoSN@C system, corresponding to the capture of $^1O_2$ by TEMP to form TEMP$-^1O_2$ [48].

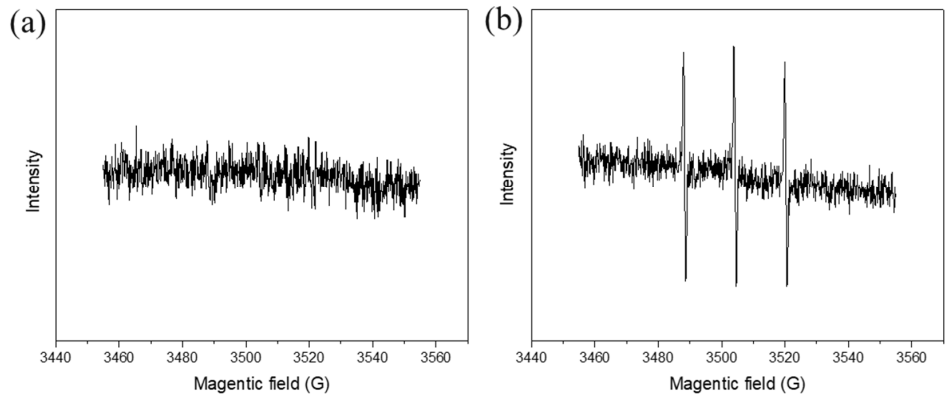

Figure 10. Identification of $^1O_2$: (**a**) EPR spectra without catalyst; (**b**) EPR spectra with catalyst.

In conclusion, the CoN@C degradation process includes the non-radical pathway to break down RhB, whereas CoSN@C employs the coordinated action of the $SO_4 \cdot^-$ and HO·radical adsorbed on the catalyst surface and non-radical path to break down RhB effectively and quickly.

4. Conclusions

- The sulfur-doped, nonhomogeneous catalyst CoSN@C was produced using a one-pot synthesis followed by carbonization, and it was employed for the degradation of RhB;
- Increasing the temperature can greatly increase the rate of RhB degradation; increasing the pH value will significantly decrease the rate of RhB degradation; the best results were achieved with 20 mg L^{-1} RhB, CoSN@C 0.05 g L^{-1}, and 1 mM PMS;
- The results of radical capture experiments and EPR tests evidenced that a large amount of $SO_4 \cdot^-$ and HO· radicals adsorbed on the catalyst surface and a certain amount of $^1O_2$ were generated in the reaction, and that the radical and non-radical pathways collaborated to degrade RhB rapidly and efficiently;
- After four cycles, the CoSN@C catalyst maintained its high catalytic activity and structural stability, and the RhB degradation rate remained at 88.9%.

Author Contributions: Conceptualization, C.Z.; methodology, C.Z. and Y.C.; software, C.Z.; validation, C.Z., Y.C. and Q.M.; formal analysis, C.Z.; resources, H.C. and J.F.; data curation, C.Z.; writing—original draft preparation, C.Z.; writing—review and editing, Y.C. and Q.M.; visualization, C.Z.; supervision, Q.M., Y.C., H.C. and J.F.; project administration, J.F.; funding acquisition, J.F. All authors have read and agreed to the published version of the manuscript.

Funding: This research was funded by State Key Laboratory of Pollution Control and Resource Reuse Foundation, grant number No. PCRRK 21003.

Institutional Review Board Statement: Not applicable.

Informed Consent Statement: Not applicable.

Data Availability Statement: Not applicable.

Conflicts of Interest: The authors declare no conflict of interest.

References

1. Ahmad, A.; Mohd-Setapar, S.H.; Chuong, C.S.; Khatoon, A.; Wani, W.A.; Kumar, R.; Rafatullah, M. Recent advances in new generation dye removal technologies: Novel search for approaches to reprocess wastewater. *RSC Adv.* **2015**, *5*, 30801–30818. [CrossRef]
2. Homaeigohar, S. The Nanosized Dye Adsorbents for Water Treatment. *Nanomaterials* **2020**, *10*, 295. [CrossRef] [PubMed]
3. Brillas, E.; Martinez-Huitle, C.A. Decontamination of wastewaters containing synthetic organic dyes by electrochemical methods. An updated review. *Appl. Catal. B Environ.* **2015**, *166*, 603–643. [CrossRef]
4. Ding, X.; Gutierrez, L.; Croue, J.-P.; Li, M.; Wang, L.; Wang, Y. Hydroxyl and sulfate radical-based oxidation of RhB dye in UV/H_2O_2 and UV/persulfate systems: Kinetics, mechanisms, and comparison. *Chemosphere* **2020**, *253*, 126655. [CrossRef] [PubMed]
5. Al-Gheethi, A.A.; Azhar, Q.M.; Kumar, P.S.; Yusuf, A.A.; Al-Buriahi, A.K.; Mohamed, R.M.S.R.; Al-shaibani, M.M. Sustainable approaches for removing Rhodamine B dye using agricultural waste adsorbents: A review. *Chemosphere* **2022**, *287*, 132080. [CrossRef]
6. Andreozzi, R.; Caprio, V.; Insola, A.; Marotta, R. Advanced oxidation processes (AOP) for water purification and recovery. *Catal. Today* **1999**, *53*, 51–59. [CrossRef]
7. Luo, Y.; Su, R.; Yao, H.; Zhang, A.; Xiang, S.; Huang, L. Degradation of trimethoprim by sulfate radical-based advanced oxidation processes: Kinetics, mechanisms, and effects of natural water matrices. *Environ. Sci. Pollut. Res.* **2021**, *28*, 62572–62582. [CrossRef]
8. Peng, J.; Wang, Z.; Wang, S.; Liu, J.; Zhang, Y.; Wang, B.; Gong, Z.; Wang, M.; Dong, H.; Shi, J.; et al. Enhanced removal of methylparaben mediated by cobalt/carbon nanotubes (Co/CNTs) activated peroxymonosulfate in chloride-containing water: Reaction kinetics, mechanisms and pathways. *Chem. Eng. J.* **2021**, *409*, 128176. [CrossRef]
9. Dai, Y.; Qi, C.; Cao, H.; Wen, Y.; Zhao, Y.; Xu, C.; Yang, S.; He, H. Enhanced degradation of sulfamethoxazole by microwave-activated peracetic acid under alkaline condition: Influencing factors and mechanism. *Sep. Purif. Technol.* **2022**, *288*, 120716. [CrossRef]

10. Qi, C.; Wen, Y.; Zhao, Y.; Dai, Y.; Li, Y.; Xu, C.; Yang, S.; He, H. Enhanced degradation of organic contaminants by Fe(III)/peroxymonosulfate process with l-cysteine. *Chin. Chem. Lett.* **2022**, *33*, 2125–2128. [CrossRef]
11. Dai, Y.; Cao, H.; Qi, C.; Zhao, Y.; Wen, Y.; Xu, C.; Zhong, Q.; Sun, D.; Zhou, S.; Yang, B.; et al. L-cysteine boosted Fe(III)-activated peracetic acid system for sulfamethoxazole degradation: Role of L-cysteine and mechanism. *Chem. Eng. J.* **2023**, *451*, 138588. [CrossRef]
12. Su, R.; Xie, C.; Alhassan, S.I.; Huang, S.; Chen, R.; Xiang, S.; Wang, Z.; Huang, L. Oxygen Reduction Reaction in the Field of Water Environment for Application of Nanomaterials. *Nanomaterials* **2020**, *10*, 1719. [CrossRef] [PubMed]
13. Qian, K.; Chen, H.; Li, W.; Ao, Z.; Wu, Y.N.; Guan, X. Single-Atom Fe Catalyst Outperforms Its Homogeneous Counterpart for Activating Peroxymonosulfate to Achieve Effective Degradation of Organic Contaminants. *Environ. Sci. Technol.* **2021**, *55*, 7034–7043. [CrossRef] [PubMed]
14. Giannakis, S.; Lin, K.-Y.A.; Ghanbari, F. A review of the recent advances on the treatment of industrial wastewaters by Sulfate Radical-based Advanced Oxidation Processes (SR-AOPs). *Chem. Eng. J.* **2021**, *406*, 127083. [CrossRef]
15. Li, X.; Huang, X.; Xi, S.; Miao, S.; Ding, J.; Cai, W.; Liu, S.; Yang, X.; Yang, H.; Gao, J.; et al. Single Cobalt Atoms Anchored on Porous N-Doped Graphene with Dual Reaction Sites for Efficient Fenton-like Catalysis. *J. Am. Chem. Soc.* **2018**, *140*, 12469–12475. [CrossRef]
16. Wei, Z.-X.; Zhu, Y.-T.; Liu, J.-Y.; Zhang, Z.-C.; Hu, W.-P.; Xu, H.; Feng, Y.-Z.; Ma, J.-M. Recent advance in single-atom catalysis. *Rare Met.* **2021**, *40*, 767–789. [CrossRef]
17. Maru, K.; Kalla, S.; Jangir, R. Dye contaminated wastewater treatment through metal-organic framework (MOF) based materials. *New J. Chem.* **2022**, *46*, 3054–3072. [CrossRef]
18. Zhong, Q.; Xu, C.; Liu, Y.; Ji, Q.; Xu, Z.; Sun, D.; Zhou, S.; Yang, B.; Dai, Y.; Qi, C.; et al. Defect-engineered FeSe2−x@C with porous architecture for enhanced peroxymonosulfate-based advanced oxidation processes. *Appl. Catal. B Environ.* **2022**, *309*, 121259. [CrossRef]
19. He, Y.; Hwang, S.; Cullen, D.A.; Uddin, M.A.; Langhorst, L.; Li, B.; Karakalos, S.; Kropf, A.J.; Wegener, E.C.; Sokolowski, J.; et al. Highly active atomically dispersed CoN_4 fuel cell cathode catalysts derived from surfactant-assisted MOFs: Carbon-shell confinement strategy. *Energy Environ. Sci.* **2019**, *12*, 250–260. [CrossRef]
20. Yang, L.; Zeng, X.; Wang, W.; Cao, D. Recent Progress in MOF-Derived, Heteroatom-Doped Porous Carbons as Highly Efficient Electrocatalysts for Oxygen Reduction Reaction in Fuel Cells. *Adv. Funct. Mater.* **2018**, *28*, 1704537. [CrossRef]
21. Mi, X.; Wang, P.; Xu, S.; Su, L.; Zhong, H.; Wang, H.; Li, Y.; Zhan, S. Almost 100% Peroxymonosulfate Conversion to Singlet Oxygen on Single-Atom CoN_{2+2} Sites. *Angew. Chem. Int. Ed.* **2021**, *60*, 4588–4593. [CrossRef] [PubMed]
22. Shang, Y.; Xu, X.; Gao, B.; Wang, S.; Duan, X. Single-atom catalysis in advanced oxidation processes for environmental remediation. *Chem. Soc. Rev.* **2021**, *50*, 5281–5322. [CrossRef] [PubMed]
23. Wang, J.; Li, B.; Li, Y.; Fan, X.; Zhang, F.; Zhang, G.; Peng, W. Facile Synthesis of Atomic Fe-N-C Materials and Dual Roles Investigation of Fe-N4 Sites in Fenton-Like Reactions. *Adv. Sci.* **2021**, *8*, 2101824. [CrossRef] [PubMed]
24. Guo, X.; Xing, T.; Lou, Y.; Chen, J. Controlling ZIF-67 crystals formation through various cobalt sources in aqueous solution. *J. Solid State Chem.* **2016**, *235*, 107–112. [CrossRef]
25. Du, X.-D.; Wang, C.-C.; Liu, J.-G.; Zhao, X.-D.; Zhong, J.; Li, Y.-X.; Li, J.; Wang, P. Extensive and selective adsorption of ZIF-67 towards organic dyes: Performance and mechanism. *J. Colloid Interface Sci.* **2017**, *506*, 437–441. [CrossRef]
26. Zhang, W.; Jiang, X.; Wang, X.; Kaneti, Y.V.; Chen, Y.; Liu, J.; Jiang, J.-S.; Yamauchi, Y.; Hu, M. Spontaneous Weaving of Graphitic Carbon Networks Synthesized by Pyrolysis of ZIF-67 Crystals. *Angew. Chem. Int. Ed.* **2017**, *56*, 8435–8440. [CrossRef]
27. Karmakar, A.; Hazra, S.; Pombeiro, A.J.L. Urea and thiourea based coordination polymers and metal-organic frameworks: Synthesis, structure and applications. *Coord. Chem. Rev.* **2022**, *453*, 214314. [CrossRef]
28. Li, X.; Ma, W.; Li, H.; Zhang, Q.; Liu, H. Sulfur-functionalized metal-organic frameworks: Synthesis and applications as advanced adsorbents. *Coord. Chem. Rev.* **2020**, *408*, 213191. [CrossRef]
29. Luo, J.; Bo, S.; An, Q.; Xiao, Z.; Wang, H.; Cai, W.; Zhai, S.; Li, Z. Designing ordered composites with confined Co–N/C layers for efficient pollutant degradation: Structure-dependent performance and PMS activation mechanism. *Microporous Mesoporous Mater.* **2020**, *293*, 109810. [CrossRef]
30. Li, N.; Li, R.; Duan, X.; Yan, B.; Liu, W.; Cheng, Z.; Chen, G.; Hou, L.A.; Wang, S. Correlation of Active Sites to Generated Reactive Species and Degradation Routes of Organics in Peroxymonosulfate Activation by Co-Loaded Carbon. *Environ. Sci. Technol.* **2021**, *55*, 16163–16174. [CrossRef]
31. Miao, J.; Geng, W.; Alvarez, P.J.J.; Long, M. 2D N-Doped Porous Carbon Derived from Polydopamine-Coated Graphitic Carbon Nitride for Efficient Nonradical Activation of Peroxymonosulfate. *Environ. Sci. Technol.* **2020**, *54*, 8473–8481. [CrossRef]
32. Cazetta, A.L.; Zhang, T.; Silva, T.L.; Almeida, V.C.; Asefa, T. Bone char-derived metal-free N- and S-co-doped nanoporous carbon and its efficient electrocatalytic activity for hydrazine oxidation. *Appl. Catal. B Environ.* **2018**, *225*, 30–39. [CrossRef]
33. Zhang, M.; Luo, R.; Wang, C.; Zhang, W.; Yan, X.; Sun, X.; Wang, L.; Li, J. Confined pyrolysis of metal-organic frameworks to N-doped hierarchical carbon for non-radical dominated advanced oxidation processes. *J. Mater. Chem. A* **2019**, *7*, 12547–12555. [CrossRef]
34. Wacławek, S.; Lutze, H.V.; Grübel, K.; Padil, V.V.T.; Černík, M.; Dionysiou, D.D. Chemistry of persulfates in water and wastewater treatment: A review. *Chem. Eng. J.* **2017**, *330*, 44–62. [CrossRef]

35. Govindan, K.; Raja, M.; Noel, M.; James, E.J. Degradation of pentachlorophenol by hydroxyl radicals and sulfate radicals using electrochemical activation of peroxomonosulfate, peroxodisulfate and hydrogen peroxide. *J. Hazard. Mater.* **2014**, *272*, 42–51. [CrossRef] [PubMed]
36. Sun, P.; Liu, H.; Feng, M.; Guo, L.; Zhai, Z.; Fang, Y.; Zhang, X.; Sharma, V.K. Nitrogen-sulfur co-doped industrial graphene as an efficient peroxymonosulfate activator: Singlet oxygen-dominated catalytic degradation of organic contaminants. *Appl. Catal. B: Environ.* **2019**, *251*, 335–345. [CrossRef]
37. Hong, Y.; Zhou, H.; Xiong, Z.; Liu, Y.; Yao, G.; Lai, B. Heterogeneous activation of peroxymonosulfate by CoMgFe-LDO for degradation of carbamazepine: Efficiency, mechanism and degradation pathways. *Chem. Eng. J.* **2020**, *391*, 123604. [CrossRef]
38. Zeng, T.; Li, S.; Hua, J.; He, Z.; Zhang, X.; Feng, H.; Song, S. Synergistically enhancing Fenton-like degradation of organics by in situ transformation from Fe_3O_4 microspheres to mesoporous Fe, N-dual doped carbon. *Sci. Total Environ.* **2018**, *645*, 550–559. [CrossRef]
39. Ji, F.; Li, C.; Deng, L. Performance of CuO/Oxone system: Heterogeneous catalytic oxidation of phenol at ambient conditions. *Chem. Eng. J.* **2011**, *178*, 239–243. [CrossRef]
40. Rastogi, A.; Al-Abed, S.R.; Dionysiou, D.D. Sulfate radical-based ferrous–peroxymonosulfate oxidative system for PCBs degradation in aqueous and sediment systems. *Appl. Catal. B Environ.* **2009**, *85*, 171–179. [CrossRef]
41. Yang, S.; Wang, P.; Yang, X.; Shan, L.; Zhang, W.; Shao, X.; Niu, R. Degradation efficiencies of azo dye Acid Orange 7 by the interaction of heat, UV and anions with common oxidants: Persulfate, peroxymonosulfate and hydrogen peroxide. *J. Hazard. Mater.* **2010**, *179*, 552–558. [CrossRef] [PubMed]
42. Lou, X.; Wu, L.; Guo, Y.; Chen, C.; Wang, Z.; Xiao, D.; Fang, C.; Liu, J.; Zhao, J.; Lu, S. Peroxymonosulfate activation by phosphate anion for organics degradation in water. *Chemosphere* **2014**, *117*, 582–585. [CrossRef] [PubMed]
43. Chen, S.; Cai, M.; Liu, Y.; Zhang, L.; Feng, L. Effects of water matrices on the degradation of naproxen by reactive radicals in the UV/peracetic acid process. *Water Res.* **2019**, *150*, 153–161. [CrossRef] [PubMed]
44. Lee, J.; von Gunten, U.; Kim, J.-H. Persulfate-Based Advanced Oxidation: Critical Assessment of Opportunities and Roadblocks. *Environ. Sci. Technol.* **2020**, *54*, 3064–3081. [CrossRef] [PubMed]
45. Gao, Y.; Wu, T.; Yang, C.; Ma, C.; Zhao, Z.; Wu, Z.; Cao, S.; Geng, W.; Wang, Y.; Yao, Y.; et al. Activity Trends and Mechanisms in Peroxymonosulfate-Assisted Catalytic Production of Singlet Oxygen over Atomic Metal-N-C Catalysts. *Angew. Chem. Int. Ed.* **2021**, *60*, 22513–22521. [CrossRef] [PubMed]
46. Zhang, L.S.; Jiang, X.H.; Zhong, Z.A.; Tian, L.; Sun, Q.; Cui, Y.T.; Lu, X.; Zou, J.P.; Luo, S.L. Carbon Nitride Supported High-Loading Fe Single-Atom Catalyst for Activation of Peroxymonosulfate to Generate (1) O_2 with 100% Selectivity. *Angew. Chem. Int. Ed.* **2021**, *60*, 21751–21755. [CrossRef]
47. Ding, Y.; Wang, X.; Fu, L.; Peng, X.; Pan, C.; Mao, Q.; Wang, C.; Yan, J. Nonradicals induced degradation of organic pollutants by peroxydisulfate (PDS) and peroxymonosulfate (PMS): Recent advances and perspective. *Sci. Total Environ.* **2021**, *765*. [CrossRef]
48. Luo, R.; Li, M.Q.; Wang, C.H.; Zhang, M.; Khan, M.A.N.; Sun, X.Y.; Shen, J.Y.; Han, W.Q.; Wang, L.J.; Li, J.S. Singlet oxygen-dominated non-radical oxidation process for efficient degradation of bisphenol A under high salinity condition. *Water Res.* **2019**, *148*, 416–424. [CrossRef]